Computational Materials Science 94 (2014) 191–197

Contents lists available at ScienceDirect

Computational Materials Science

journal homepage: www.elsevier.com/locate/commatsci

Crystal plasticity finite element simulation of crack growth in single crystals

J. Li [a,*], H. Proudhon [a], A. Roos [b], V. Chiaruttini [b], S. Forest [a]

[a] MINES ParisTech, Centre des matériaux, CNRS UMR 7633, Evry, France
[b] ONERA, The French Aerospace Lab, Châtillon, France

ARTICLE INFO

Article history:
Received 15 December 2013
Received in revised form 24 March 2014
Accepted 27 March 2014
Available online 10 May 2014

Keywords:
Crystal plasticity
Finite element
Crack propagation
Adaptive remeshing
Single crystals

ABSTRACT

A new method for 3D simulation of crack growth in single crystals is proposed. From Crystal Plasticity Finite Element (CPFE) computations of a pre-cracked single crystal, a damage indicator based on the accumulated slip, the resolved shear stress and the normal stress on each slip system is calculated at each integration point and for every time increment. The crack growth direction is then determined in 3D by analysing the damage indicator in the region around the crack front. The crack is extended via remeshing at each propagation event. At this point the CPFE computation is restarted, using the new crack configuration. Two examples in BCC single crystals featuring different crystal orientations and slip systems show the crack propagation simulations under monotonic loading over distances comparable to the crystal size and with non-regular crack shape and path.

1. Introduction

In many industrial cases, the major part of the total fatigue-life of structural components is spent in the regime of initiation and micro-propagation of small cracks. During small fatigue crack growth, the shape and growth rate directly depend on microstructural features. Microstructure-based models of fatigue-life prediction were proposed by [1–4], where accumulated plastic slip, resolved shear stress or normal stress to slip planes were supposed to cause crack initiation. The damage variables based on these models were simulated and compared in [5]. However, to date, reliable prediction of 3D small fatigue crack growth paths in metallic polycrystalline materials remains a challenge.

Different numerical methodologies currently exist to simulate fatigue crack propagation in 3D. The X-FEM approach is one of the most popular methods in Linear Elastic Fracture Mechanics (LEFM) without remeshing [6]. Although it was extended to elasto-plastic fracture mechanics, there are still many technical issues to be resolved. An alternative methodology is the Cohesive Zone approach [7]. However, the crack path must usually be known in advance which limits greatly the prediction of complex paths. Continuum damage mechanics can also be used, but it remains computationally expensive [8,9].

The objective of this paper is to introduce a new methodology to simulate efficiently crack propagation in 3D single crystals. CPFE computations coupled with a post-processing procedure are used to determine the direction of crack growth and to remesh the crack surface adaptatively at each crack propagation event [10]. The damage indicator, which is based on a combination of resolved shear stress and normal stress with respect to the slip plane, and accumulated plastic slip, is computed and evaluated at the crack front for each load increment.

In Section 3, the methodology is presented and showcased on a single crystal with only one slip system loaded in tension. An example of a single crystal with 12 slip systems is presented in Section 4, under tensile loading. The final section presents a discussion and conclusions.

2. Experimental studies

The material of interest is a near beta titanium alloy VST55531 with a B.C.C. crystal structure. The average grain size is 65 μm. The in situ fatigue experiments were carried out at the ESRF (France) using a triangular prismatic pre-cracked sample under load control (not presented here). The maximum loading amplitude corresponds to a tensile stress of 500 MPa. The stress ratio $\sigma_{max}/\sigma_{min}$ is 0.1. The growth of fatigue crack surfaces in the polycrystalline sample was characterised by X-ray tomography every 2000 cycles [11]. It was observed that cracks initiated from the notch after 28,000 cycles. The average crack growth rate for the first grains crossed by the crack was about 1 nm per cycle. Thus, at each stage of observation, cracks typically propagated over 2 μm and mainly intragranularly along {1 1 2} and {1 1 0} crystallographic planes of

* Corresponding author. Tel.: +33 1 60 76 30 67; fax: +33 1 60 76 31 50.
E-mail address: jia.li@mines-paristech.fr (J. Li).

http://dx.doi.org/10.1016/j.commatsci.2014.03.061
0927-0256/

the BCC structure. After 46,000 cycles, cracks propagated into the neighbouring grains.

3. Constitutive model and crack growth methodology

3.1. Proposed methodology for crack propagation

In this section, the crack growth methodology is presented on a simplified test case, as shown in Fig. 1. It consists of $[1\,1\,\bar{1}](1\,1\,2)$ single slip crystal, in which the initial crack plane is perpendicular to the loading direction and the slip plane is oriented at an angle of 54.7° with respect to the crack plane, see Fig. 2(b). In Section 4, the method is applied to a single crystal with a crystal orientation measured by X-ray diffraction during the in situ tomographic experiment, in which all the 12 $\langle 1\,1\,1\rangle\{1\,1\,0\}$ slip systems can be activated. The maximum loading applied in the simulations is the same as in the experiments. However, in these simple examples, the CPFE computations are performed under monotonic loading instead of fatigue loading because the methodology remains to be applied to complex loading.

Fig. 1 shows the main steps of the crack growth simulation methodology. For each CPFE computation, the damage indicator is computed at all integration points. Then, a post-processing procedure is carried out at the preset increment to evaluate the damage indicator around the crack front, on a set of planes orthogonal to the crack front. For each such plane, the origin is defined at its intersection with the crack front. Then, the crack growth direction is selected as pointing from the origin to the location where the damage indicator is the maximum, at a preset distance R_0 from the origin. The crack growth distance R_0 is fixed as 2 μm in both examples, which corresponds to the average experimentally measured crack growth distance. The parameter R_0 is related to material properties, loading amplitude and other experimental conditions. The set of propagation directions along the front is used to create the geometry of the crack propagation area, which is then inserted into the FE mesh of the single crystal, as will be explained in detail in Section 3.4. Then, a new CPFE computation is carried out with the same loading conditions as before. In this paper, to illustrate the methodology, the procedure is repeated until the whole single crystal is broken.

The initial Finite Element (FE) mesh is a pre-cracked single crystal with a rectangular crack, as shown in Fig. 2(a). The FE mesh is generated by inserting a crack surface mesh into a single crystal mesh using Z-cracks [15], which is a module of the Z-set FE software [13]. The insertion procedure is performed by creating the intersection points and edges of the two meshes and then remeshing the whole mesh. The size of the single crystalline cube is $100 \times 100 \times 100\ \mu m^3$, which approximately corresponds to the size of the grain in which the pre-crack is presented in the experimental polycrystalline sample.

Regarding the boundary conditions, according to the loading applied in the in situ experiments, a displacement of 0.5 μm is applied monotonically in a time interval of 1 s at the top surface in the vertical tensile direction z, and vertical displacement is blocked at the bottom surface, so that the loading rate $\dot{\varepsilon}_{zz} = 5 \times 10^{-3}\ s^{-1}$. Detailed boundary conditions are shown in Fig. 2(a). For the single slip crystal, symmetry conditions in the y direction are applied at the back and the front surface to minimise the free surface effect. In the case of 12 slip systems crystal in Section 4, these surfaces are free of forces since the prediction of free surface effects on cracking and simulation of curved cracks also belong to the objective of this work.

3.2. Crystal plasticity model

In order to analyse the slip system activity and to determine the driving force for short crack propagation, an elasto–visco-plastic crystal plasticity model was selected [12]. The CPFE computations were carried out in the framework of infinitesimal strains using the

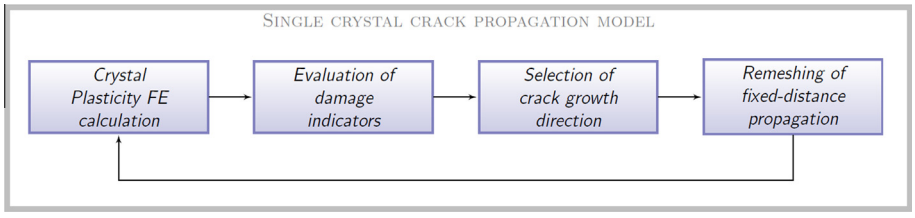

Fig. 1. Crack propagation simulation methodology.

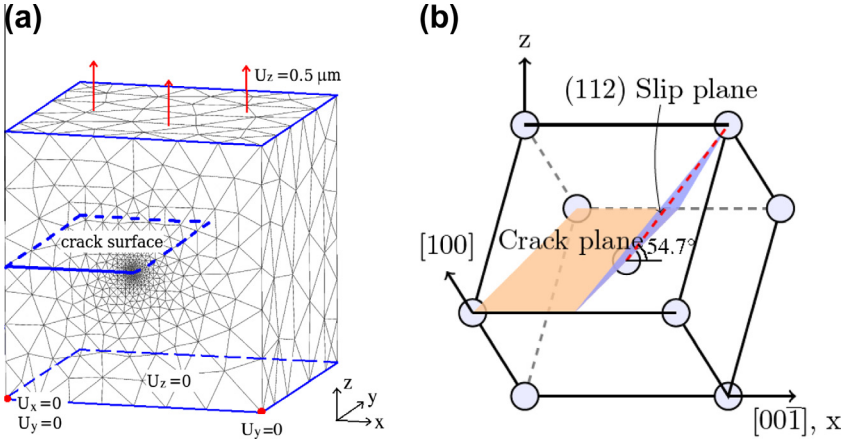

Fig. 2. (a) FE mesh of the pre-cracked single crystal and the applied boundary conditions. The dimension of the mesh is 100 μm^3. (b) Schematic representation of the crystal orientation and the single slip system $[1\,1\,\bar{1}](1\,1\,2)$ of the example in Section 3.

Z-set software [13], because in the experiments only small deformations were observed at the crack front.

The total strain tensor $\underset{\sim}{\boldsymbol{\varepsilon}}$ is partitioned into an elastic part $\underset{\sim}{\boldsymbol{\varepsilon}}^e$ and a plastic part $\underset{\sim}{\boldsymbol{\varepsilon}}^p$. Regarding elasticity, the material is considered linear and isotropic for simplicity, according to Hooke's law:

$$\underset{\sim}{\boldsymbol{\varepsilon}}^e = \frac{1+\nu}{E}\underset{\sim}{\boldsymbol{\sigma}} - \frac{\nu}{E} tr(\underset{\sim}{\boldsymbol{\sigma}})\,\underset{\sim}{1}, \tag{1}$$

with $\underset{\sim}{1}$ the second-order identity tensor, the Young modulus $E = 110$ GPa and the Poisson ratio $\nu = 0.3$.

The plastic strain is the result of N potentially active slip systems s, only one slip system in Section 3 and 12 $\langle 1\,1\,1\rangle\{1\,1\,0\}$ slip systems in Section 4, according to

$$\dot{\underset{\sim}{\boldsymbol{\varepsilon}}}^p = \sum_{s=1}^{N} \dot{\gamma}^s \underset{\sim}{\boldsymbol{m}}^s, \tag{2}$$

where $\underset{\sim}{\boldsymbol{m}}^s$ is the orientation tensor defined by the slip plane normal $\underline{\boldsymbol{n}}^s$ and the slip direction $\underline{\boldsymbol{l}}^s$ of each system s, and $\dot{\gamma}^s$ is the slip rate defined by a power law:

$$\underset{\sim}{\boldsymbol{m}}^s = \frac{1}{2}(\underline{\boldsymbol{n}}^s \otimes \underline{\boldsymbol{l}}^s + \underline{\boldsymbol{l}}^s \otimes \underline{\boldsymbol{n}}^s), \tag{3}$$

$$\dot{\gamma}^s = sign(\tau^s)\left\langle \frac{|\tau^s| - \tau_0}{K} \right\rangle^n, \tag{4}$$

with parameters $K = 300$ MPa $s^{1/n}$ and $n = 3$. The critical resolved shear stress $\tau_0 = 300$ MPa and $\tau^s = \sigma : m^s$ is the shear stress resolved on slip system s. For simplicity no hardening is introduced in this model.

3.3. Damage indicator

During fatigue loading of the pre-cracked sample, plastic deformation occurs near the crack tip due to the dislocation movements along the slip planes. This mechanism is described by the slip γ^s on each slip systems s in the crystal plasticity model. When the crack propagates, the tomographic observation of the 3D fatigue crack surface of the VST55531 sample reveals that the crack propagates on crystallographic planes. This stage is governed by the mode II loading and driven by the resolved shear stress τ^s, as explained in [14]. In addition, it was demonstrated that the normal stress σ_n^s acting on the slip planes could also influence the nucleation and the short crack propagation [3]. Therefore, in this work a damage indicator that is the combination of γ^s, τ^s and σ_n^s is retained. Previously, a similar form was proposed by [3,4]. Here, at each integration point the damage indicator D at time t is the maximum value among the slip systems s, according to

$$D(t) = \max_s \int_0^t |\dot{\gamma}^s|(|\tau^s| + k\langle\sigma_n^s\rangle)\mathrm{d}t, \tag{5}$$

with k a material parameter set to 0.4 as in [4]. This value is found by fitting the uniaxial data against the pure torsion data. It enforces the role of normal stress in D.

3.4. Crack growth direction

The damage indicator $D(t)$ is computed during the CPFE calculation. Then, the direction of crack growth is determined using a post-processing procedure. For this, a set of circles of preset radius R_0 lying in normal planes along the crack front is defined. These circles are centered at the control points on the crack front. The damage indicator D is interpolated along these circles, and for each circle the location of its maximum value is determined. The crack propagation direction is then taken as the one going from the corresponding control point to that location. A corresponding propagation angle θ between the propagation direction and the local crack plane orientation is also determined.

During the numerical procedure, a smoothed crack front is computed [16]. This approximated smooth crack front Γ is composed of $i+1$ equidistant points on the initial crack front, see Fig. 3. These nodes are called control points $P_k (0 \leqslant k \leqslant i)$ that do not necessarily correspond to the real mesh nodes. The precision of the approximation can be controlled by the number of control points i. According to a numerical analysis in [16], i should be larger than 1/16 of the number of nodes on the initial crack front. Any point at the approximated crack front Γ is then modeled as an oriented regular curve $\underline{\boldsymbol{P}}(a)$, with $a \in [0; a_{max}]$ the curvilinear parameter and a_{max} is the maximum length of $\underline{\boldsymbol{P}}(a)$.

Then, a local orthonormal coordinate basis associated to $\underline{\boldsymbol{P}}(a)$ is computed, which contains the tangent vector or $\underline{\boldsymbol{T}}(a)$, written as [16]

$$\underline{\boldsymbol{T}}(a) = \left\| \frac{d\underline{\boldsymbol{P}}(a)}{da} \right\|^{-1} \frac{d\underline{\boldsymbol{P}}(a)}{da}, \tag{6}$$

and the vector $\underline{\boldsymbol{N}}(a)$, defined as

$$\underline{\boldsymbol{N}}(a) = \underline{\boldsymbol{B}}(a) \wedge \underline{\boldsymbol{T}}(a), \tag{7}$$

with $\underline{\boldsymbol{B}}(a)$ the normal vector. In order to calculate $\underline{\boldsymbol{B}}(a)$, for any $a \in [0; a_{max}]$, an auxiliary vector $\underline{\widehat{\boldsymbol{B}}}(a)$ is introduced as a linear interpolation between $\underline{\widehat{\boldsymbol{B}}}_k$ and $\underline{\widehat{\boldsymbol{B}}}_{k+1}$, as follows:

$$\underline{\widehat{\boldsymbol{B}}}(a) = (1-u)\underline{\widehat{\boldsymbol{B}}}_k + u\underline{\widehat{\boldsymbol{B}}}_{k+1}, \tag{8}$$

with $u = (a_{k+1} - a)/(a_{k+1} - a_k)$. As shown in Fig. 3, the $\underline{\widehat{\boldsymbol{B}}}_k$ vector are set up at each control point P_k as vector normal to the crack surface element that is nearest to P_k. The orientation of $\underline{\widehat{\boldsymbol{B}}}_k$ is such that $\underline{\widehat{\boldsymbol{B}}}_k \wedge \underline{\boldsymbol{T}}(a)$ is oriented inside the material, into which the crack propagates. Thus, the normal vector $\underline{\boldsymbol{B}}(a)$ is written as:

$$\underline{\boldsymbol{B}}(a) = \frac{\underline{\widehat{\boldsymbol{B}}}(a) - (\underline{\widehat{\boldsymbol{B}}}(a) \cdot \underline{\boldsymbol{T}}(a))\underline{\boldsymbol{T}}(a)}{\|\underline{\widehat{\boldsymbol{B}}}(a) - (\underline{\widehat{\boldsymbol{B}}}(a) \cdot \underline{\boldsymbol{T}}(a))\underline{\boldsymbol{T}}(a)\|}, \tag{9}$$

With this local orthonormal basis, all the points situated at the circle of radius R_0 around each control points can be defined.

Alternatively, the growth distance could be evaluated from the distribution of D along the crack growth direction θ. This would be particularly useful to define a threshold of D by comparing with experimental measurements, in future work.

For a single crystal with one slip system $[1\,1\,\bar{1}](1\,1\,2)$ oriented in such a manner that the crack plane is $(0\,0\,1)$ and the crack front is $[\bar{1}\,1\,0]$, see Fig. 2(b), Fig. 4(a) shows D along the circles of interest at different depths along the crack front, which lies along the y-axis. The different depths are represented by the different colours. The crack tip is at the center of the figure. Two branches of D appear, respectively at $\theta = 63^\circ$ and $\theta = 320^\circ$. In order to determine the direction of the crack propagation, the value of D is plotted along these two directions for up to 4 μm from the crack tip, see Fig. 4(b). For a given distance $R_0 = 2$ μm, the value along the direction of $\theta = 63^\circ$ is higher than that of $\theta = 320^\circ$. Therefore, $\theta = 63^\circ$ is selected as the crack growth direction. It can be observed that, for a mesh size chosen appropriately near the crack front, the crack growth direction does not change with R, at least in a given range of R values. The crack growth distance of 2 μm corresponds to approximately 3 elements of the FE mesh.

3.5. Remeshing

Once the crack growth direction for each control point has been determined, a new crack front is generated using the preset crack growth distance R_0. The surface of the crack extension is built using the initial and the new crack fronts. The 3D crack propagation is obtained by inserting the extension crack surface into the single

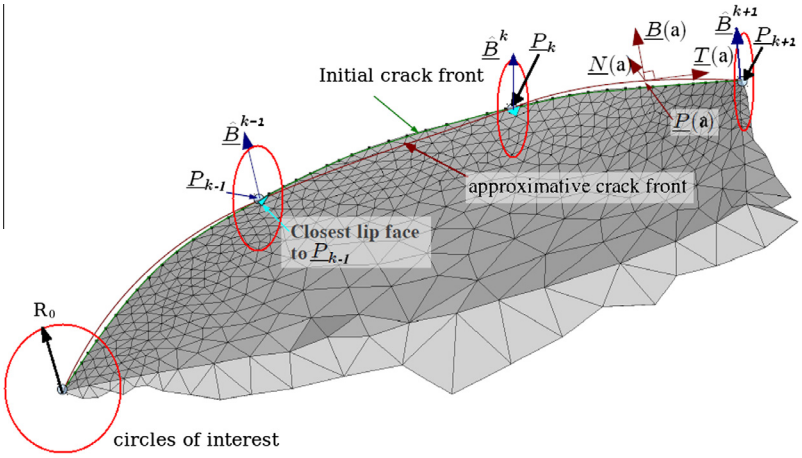

Fig. 3. Schematic representation of initial crack front, approximative crack front Γ, control points P_k, local orthonormal coordinate basis and the circles of interest of preset radius R_0, that is the distance of crack growth, along Γ centered at control points on normal planes to the crack front, edited from [16].

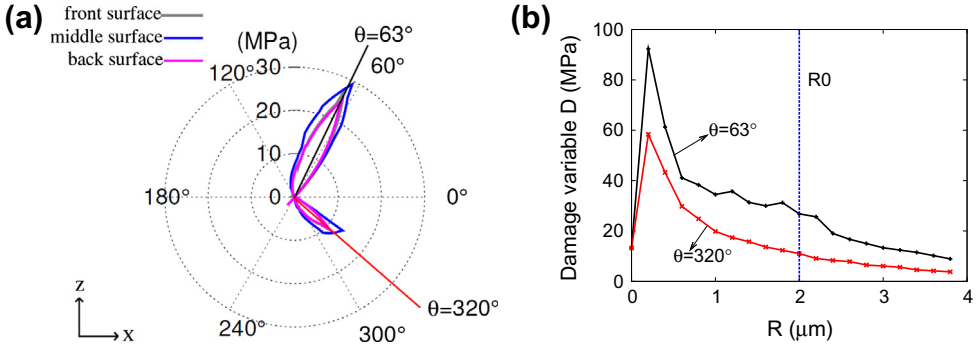

Fig. 4. (a) The damage indicator D ($t = 1$ s) around the crack tip on the xz plane interpolated to the circles of interest of radius of 2 μm on different depths below the surface (represented by different colours). (b) The value of D ($t = 1$ s) along two directions at $\theta = 63^\circ$ and $\theta = 320^\circ$ at the front surface. (For interpretation of the references to colour in this figure legend, the reader is referred to the web version of this article.)

crystal mesh with the Z-cracks software. Detailed information about the crack surface extension procedure is described in [16]. Next, a new CPFE computation is started with the new FE mesh. Then, the whole routine is carried out again, as shown in Fig. 1.

Currently, the mechanical fields are not transferred from the initial mesh to the new one after remeshing, so the accumulated plastic strain is lost from one step to the next. This is because the FE software cannot do that yet in a parallel mode, as required for large scale 3D computations. This is the reason why the new computation is started from the beginning for the same loading conditions with the new crack configuration.

However, a preliminary simulation with transferred variables is performed to evaluate the impact on crack growth direction. A tension–compression load is applied to the pre-cracked single

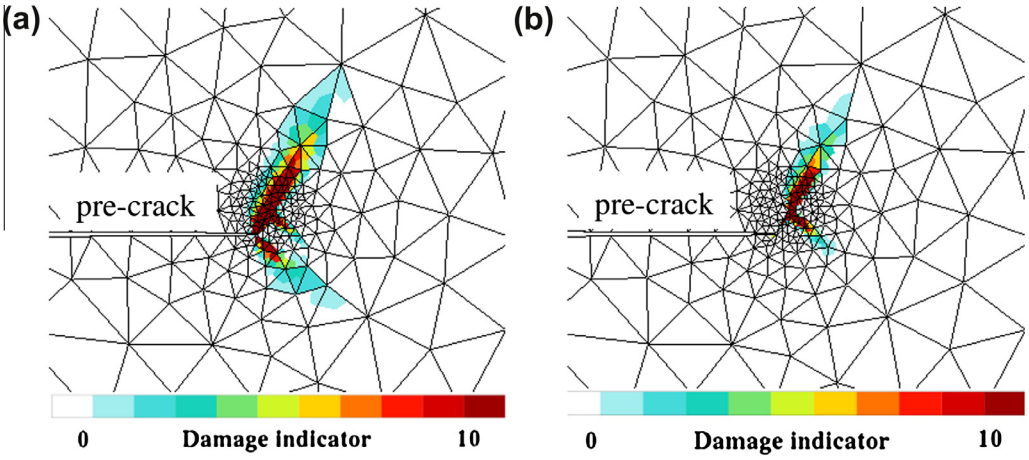

Fig. 5. Front view of the sample with damage indicator D (in MPa) at the crack tip (a) with transferred internal variables at $t = 1$ s, (b) without transferred internal variables at $t = 1$ s.

crystal. After the first crack propagation event, the state variables are transferred to the new mesh and treated as the initial state of the second CPFE computation. Fig. 5(a) shows the result of the second CPFE computation, i.e. initialised with the transferred variables. Compared to the simulation without field transfer, in Fig. 5(b), the interpolated value of D to the circles increases slightly in the direction of $\theta = 320°$. However, the direction of crack propagation remains the same at this step. Ultimately, transferring state variables will be done in the future calculations on polycrystalline agregates, but this does not change the global methodology nor the results presented in this paper. This is related to the 2 μm propagation length, a distance where the accumulated plastic activity is rather small.

3.6. Crack propagation results

Fig. 6 shows an intermediate stage among the 32 crack propagation events of the crack propagation in the single slip single crystal at $t = 1$ s. One can see that a crack bifurcation occurs after 8 μm of crack propagation, i.e. 4 crack propagation events. The location of crack bifurcation is controlled by the parameter k in Eq. 5. Another calculation with k set to zero showed that the crack bifurcation did not take place. However, this kind of crack bifurcation along the kink band direction exists also in fatigue experiments. Then the crack continues upwards, in the same direction as the first steps,

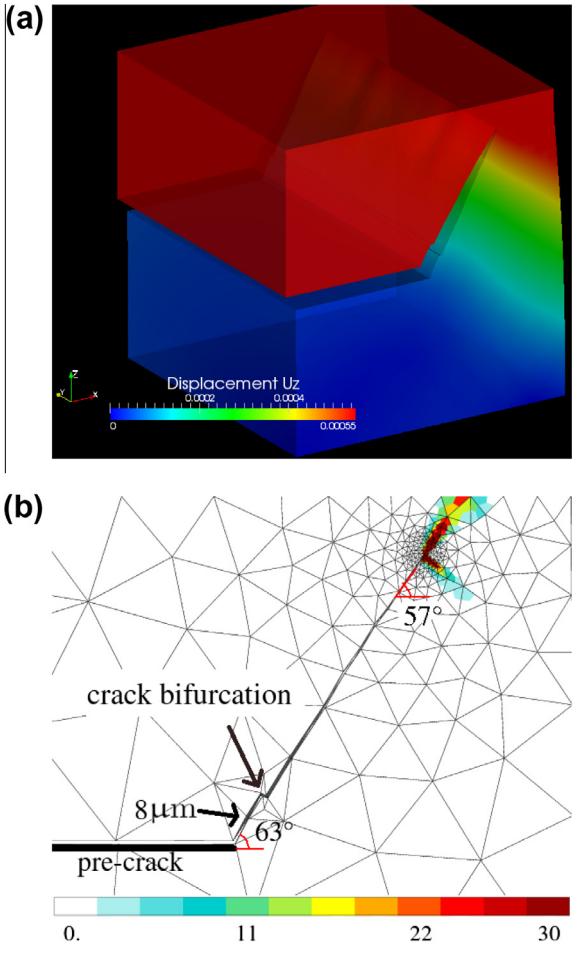

Fig. 6. Crack propagation in a single crystal with single slip system. (a) The displacement field in the tensile direction (in mm). The mesh deformation is magnified by a factor 10 for better visualisation. (b) The damage indicator D (in MPa). A detailed view of the step by step propagation is available in the supplementary material of this article.

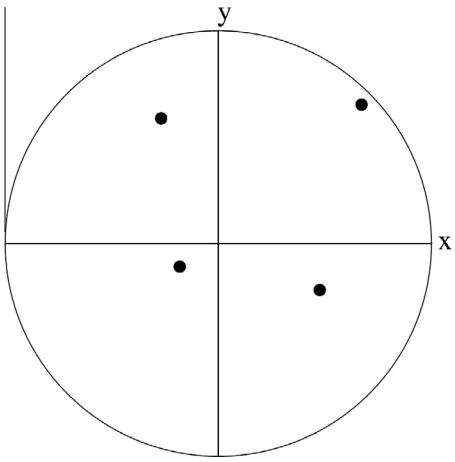

Fig. 7. {1 1 1} pole figure showing the crystal orientation $\phi_1 = 142.8°$, $\psi = 32.0°$, $\phi_2 = 214.4°$ from one grain of the polycrystalline sample, using the Bunge convention, as measured by X-ray diffraction. The axes x and y correspond to the coordinate axes of Fig. 9(a).

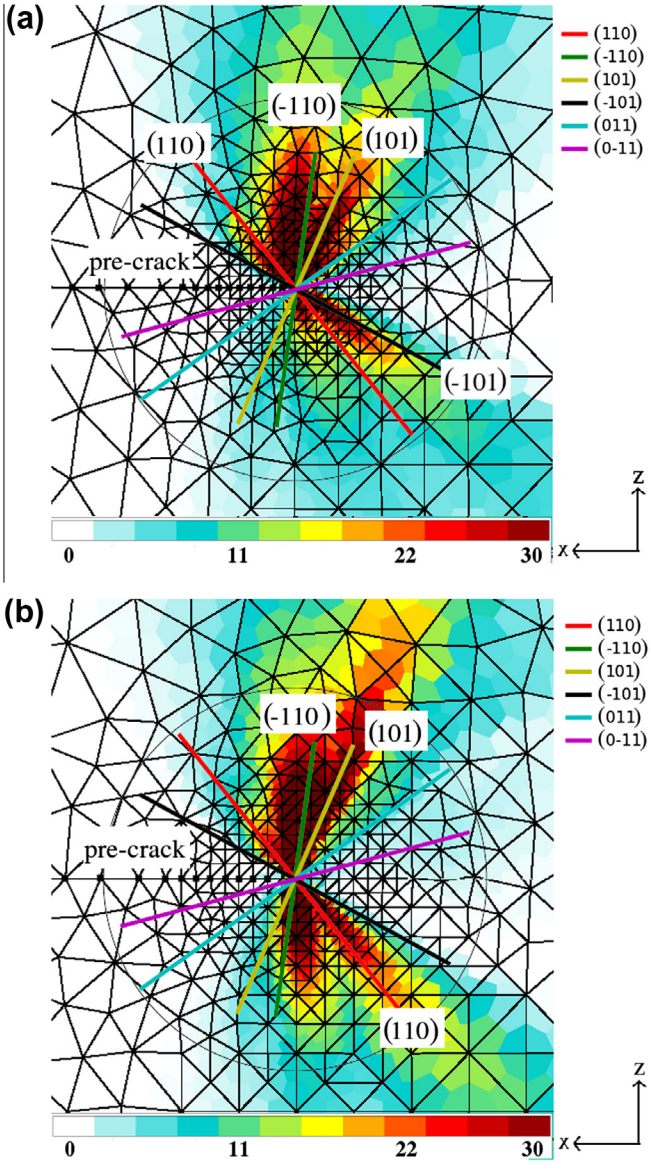

Fig. 8. The damage indicator D (in MPa) and slip plane traces at the crack tip at the front surface (a) and the back surface (b) of the single crystal.

until the crystal is completely broken. The direction of crack propagation decreases progressively from 63° at the beginning to 56° due to the equilibrium of structure and the free boundaries. It can be observed that the crack growth direction is not exactly along the slip plane, oriented at an angle of 54.7° with respect to the horizontal direction, see Fig. 2(b). As a result, the crack surface does not exactly coincide with a definite crystallographic plane.

A mesh sensitivity analysis is also carried out in order to find a reasonable element size with respect to the distance of crack growth R_0. For the first crack propagation event in the single slip crystal, the analysed element sizes near the crack front are 0.1 μm, 0.4 μm, 0.6 μm and 0.8 μm. The interpolated variables along the circles and the crack growth direction are identical for every simulation except for the element size of 0.8 μm. Thus, for the single slip crystal, the element size is chosen as 0.6 μm at the crack front. For the single crystal with 12 slip systems, presented in the next section, the minimum element size is 0.1 μm at the crack front, which is required due to the complexity of slip system activity.

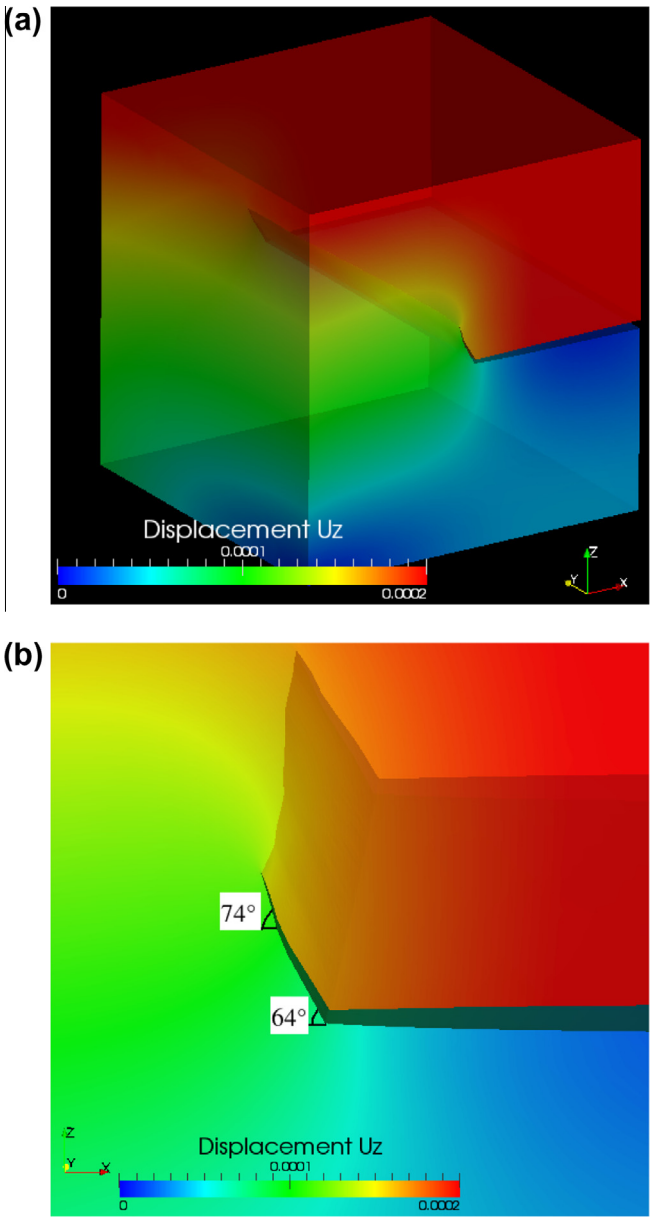

Fig. 9. A intermediate step of crack propagation in the 12 slip systems single crystal. (a) The displacement field in the tensile direction (in mm). The mesh deformation is magnified by a factor 10 for better visualisation. (b) A closer view of the crack tip at the same instant.

4. Crack propagation results for 12 slip systems

In this section, a simulation of crack propagation in a single crystal with 12 $\{1\,1\,0\}\langle 1\,1\,1\rangle$ slip systems is considered. The crystal orientation is a real grain orientation from one grain of the polycrystalline sample in which an initial crack is introduced, see Fig. 7. The crack propagation distance is $R_0 = 2$ μm. The coordinate system is shown in Fig. 9(a). The CPFE simulations are performed on a computing node with 32 CPU cores and 256 Gb memory. The initial single crystal mesh with 12 slip systems features 5×10^6 degree of freedom (DOF). Using a multithreaded computation with 32 threads, the CPU time of the CPFE computation including the damage indicator integration is approximately 40 h.

After the first CPFE computation with a pre-cracked FE mesh similar to Fig. 2(a), the analysis of the damage indicator field and the traces of slip planes at the crack front are shown in Fig. 8(a and b) at the front and the back surfaces of the single crystal respectively. It can be seen that the maximum values of the damage indicator mainly located along the traces of the $(\bar{1}\,0\,1)$, $(1\,1\,0)$, $(1\,0\,1)$ and $(\bar{1}\,1\,0)$ slip planes. Due to the crystal orientation, it is not the same between the front and back surfaces.

The analysis of damage indicator shows that the maximum values of D at the front and the back surfaces are along the plane $(1\,0\,1)$ with an angle of 64° with respect to the horizontal direction. At the second crack propagation event, the crack continues in the same direction. However, at the third event, the influence of the $(\bar{1}\,1\,0)$ plane becomes important at the back surface. Therefore, the crack changes growth direction there. It propagates on a combination of $(1\,0\,1)$ and $(\bar{1}\,1\,0)$ planes. Fig. 9 shows a back view of the displacement field of an intermediate crack propagation. Between the front and the back surfaces, the crack growth direction changes progressively.

5. Conclusions

In this work, a method of crack propagation simulation in single crystals has been developed in this work. Two simulations with a single slip crystal and a 12 slip systems crystal show that the approach can simulate 3D crack propagation over distances comparable to the crystal size and variation of crack planes during growth. This method presents several advantages: (i) It is a computationally efficient method. Compared to the CPFE computational time, the time it takes to interpolate the damage indicator to the circles, and to select a crack growth direction and remeshing is only a few minutes. Thus, the computational time is essentially determined by the CPFE time. (ii) Crack front fragmentation and bifurcation can be simulated. (iii) The physically based damage indicator can easily be modified by comparing with experimental measurements. However, there remain several major limitations: (i) the crack growth rate is not simulated in the present work. Threshold values should be defined for the damage indicator D. (ii) The CPFE computations are performed in the small deformation framework. (iii) Regarding robustness of this method, the minimum element size around the crack tip depends on the given crack propagation distance.

For future work, the stress and strain field transfer during a crack propagation event will be performed, so that the plastic history is preserved, and also to avoid the computationally expensive restarts. By analysing the slip activity and damage indicator values of the single crystal with 12 slip systems at different depths along the crack front, the crack growth rate can be determined by choosing a threshold of the damage indicator. Then, the whole procedure will be applied to the simulation of polycrystalline materials under

fatigue loading [17]. The crack growth direction and the rate of crack propagation will be simulated and compared to the experimental measurements.

Acknowledgement

This work is being carried out under the French ANR Project CRYSTAL 2010-BLAN-91801.

Appendix A. Supplementary material

Supplementary data associated with this article can be found, in the online version, at http://dx.doi.org/10.1016/j.commatsci.2014.03.061.

References

[1] D.L. McDowell, K. Gall, M.F. Horstemeyer, J. Fan, Eng. Fract. Mech. 70 (2003) 49–80.
[2] D.L. McDowell, F.P.E. Dunne, Int. J. Fatigue 32 (2010) 1521–1542.
[3] A. Fatemi, D.F. Socie, Fatigue Fract. Eng. Mater. Struct. 11 (3) (1988) 149–165.
[4] K. Dang-Van, Adv. Multiaxial Fatigue, ASTM (1191) (1993) 120–130.
[5] J.D. Hochhalter, D.J. Littlewood, R.J. Christ Jr., M.G. Veilleux, J.E. Bozek, A.R. Ingraffea, A.M. Maniatty, Model. Simul. Mater. Sci. Eng. 18 (2010) 045004.
[6] E. Bechet, H. Minnebo, N. Moës, B. Burgardt, Int. J. Numer. Methods Eng. 64 (2005) 1033–1056.
[7] G.I. Barenblatt, Adv. Appl. Mech. 7 (1962) 55–129.
[8] O. Aslan, S. Forest, Comput. Mater. Sci. 45 (2009) 756–761.
[9] K. Saanouni, M. Hamed, Int. J. Solids Struct. 50 (2013) 2289–2309.
[10] V. Chiaruttini, D. Geoffroy, V. Riolo, M. Bonnet, Eur. J. Comput. Mech. 21 (2012) 208–218.
[11] M. Herbig, A. King, P. Reischig, H. Proudhon, E.M. Lauridsen, J. Marrow, J.-Y. Buffière, W. Ludwig, Acta Mater. (59) (2011) 590–601.
[12] L. Meric, G. Cailletaud, J. Eng. Mater. Technol. 113 (1991) 171–182.
[13] http://www.zset-software.com.
[14] A. Cheng, C. Laird, Mater. Sci. Eng. 60 (1983) 177–183.
[15] http://www.zset- software.com/products/z-cracks/.
[16] V. Chiaruttini, J. Guilie, V. Riolo, M. Bonnet, Fast and Efficient Stress Intensity Factors Computations for 3D Cracked Structures Application to Unstructured Conform Meshes or X-FEM Discretization, in preparation.
[17] S. Flouriot, S. Forest, L. Remy, Comput. Mater. Sci. 26 (2003) 61–70.